Journal of Materials Chemistry A

COMMUNICATION

View Article Online
View Journal | View Issue



Cite this: J. Mater. Chem. A, 2018, 6, 19947

Received 7th July 2018
Accepted 27th September 2018

DOI: 10.1039/c8ta06510a

rsc.li/materials-a



# Polymer solar cell textiles with interlaced cathode and anode fibers†

Peng Liu,‡[a] Zhen Gao,‡[a] Limin Xu,[a] Xiang Shi,[a] Xuemei Fu,[a] Ke Li,[b] Bo Zhang,[a] Xuemei Sun [a] and Huisheng Peng *[a]

To produce next generation flexible electronics, a lot of effort has been made to develop organic photovoltaic textiles that may deform in three dimensions and that are also breathable from fiber-shaped polymer solar cells where the cathode and anode fibers are twisted together. However, a desired organic photovoltaic textile has not been realized at an applicable size, because it is challenging or even impossible to effectively connect a large amount of twisted fiber electrodes in it. Herein, through the design of an interlaced structure of cathode and anode fibers, we have realized expected organic photovoltaic textiles at the applicable scale of meters for the first time using an industrial loom. This novel structure has successfully integrated the device fabrication, textile weaving and circuit connection all in one process, which significantly enhances the performance of the organic photovoltaic textiles and facilitates their commercialization. The polymer solar cell textiles were thin, lightweight and flexible with high working stability, and were very close to materials used for daily clothes, affording them potential in a variety of emerging new application fields such as wearable electronics, biomedical electronics and artificial intelligence.

With the rapid development of wearable electronics, the requirement for a sustainable and flexible power system has become increasingly urgent.[1–8] Flexible solar cells, which can harvest clean and renewable solar energy, show great potential in a variety of fields such as wearable electronics and thus draw a lot of academic attention.[9–13] Among all types of solar cell, polymer solar cells demonstrate advantages of light weight, low cost, easy fabrication, *etc.* In particular, the intrinsic flexibility of the polymer active layer makes these materials more favorable for fabrication into flexible devices than their inorganic counterparts.[14–17] Polymer solar cells are generally made into thin films to achieve the desired flexibility.[18,19] However, strictly speaking, thin-film polymer solar cells are typically bendable, not flexible in three dimensions allowing them to bear more complex and severe deformations such as twisting. In other words, thin-film polymer solar cells may fatigue or even fail to work during applications where a variety of deformations including twisting may occur. Besides, from the perspective of wearable applications, it is hard for film polymer solar cells to intimately make contact with curvilinear surfaces like the human body.[20] Furthermore, when a thin-film polymer solar cell is worn on our bodies, it prevents the permeation of air and moisture and thus makes us uncomfortable.

In recent years, a lot of attention has been paid to making organic photovoltaic textiles that may deform in three dimensions and are breathable to simultaneously solve the above bottleneck problems with many promising advantages in various applications including wearable electronics and biomedical electronics.[21–24] Generally, a fiber-shaped polymer solar cell is composed of two fiber electrodes twisted with each other, and one of them is coated with multiple functional layers like buffer and active layers (Fig. S1†).[21,25] However, until now, it has remained difficult to weave these fiber-shaped polymer solar cells into organic photovoltaic textiles at an applicable size. The bottleneck lies in the fact that it is challenging or even impossible to effectively connect a large amount of twisted fiber electrodes of the constructed fiber-shaped polymer solar cells into an organic photovoltaic textile using typical assembly methods like welding.[26] This problem severely restricts the further development of organic photovoltaic textiles and needs to be solved urgently.

Here, we have invented an interlaced structure to fabricate polymer solar cell textiles to make the circuit connection much easier. For the first time, it is possible and efficient to produce polymer solar cell textiles at the applicable scale of meters using an industrial loom. As shown in the illustration of the polymer solar cell textile, it can be designed into modules connected in series or parallel (Fig. 1a). Each module contains an interlaced

[a]State Key Laboratory of Molecular Engineering of Polymers, Department of Macromolecular Science, Laboratory of Advanced Materials, Fudan University, Shanghai 200438, China. E-mail: penghs@fudan.edu.cn

[b]BASF Advanced Chemicals Company Limited, Shanghai 200137, China

† Electronic supplementary information (ESI) available. See DOI: 10.1039/c8ta06510a

‡ The first two authors contributed equally to this work.

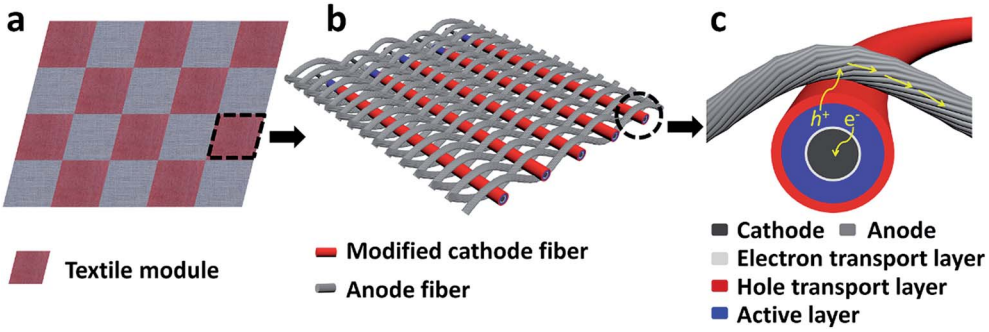


Fig. 1 Schematic illustration of the polymer solar cell textile (a), one module in the textile (b), and the intersection of the cathode and anode fibers (c).

structure from the warp and weft yarns in the organic photovoltaic textile (Fig. 1b). Clearly, the warp yarns can be easily connected to each other, and the weft yarns are also easily connected together. The above warp and weft yarns serve as the anode and modified cathode in the polymer solar cell textile, respectively. Therefore, they may be effectively connected to power the external electronic product.

Taking a closer look at the microstructure and working mechanism of this polymer solar cell textile, the holes generated at the active layer under solar irradiation transport to the anode fibers and electrons transport to the cathode fibers (Fig. 1c). This interlaced structure leads to the series connection of modified cathode fibers along the weft direction and parallel connection along the warp direction of the anode fibers. Therefore, the output voltage and current in the organic photovoltaic textile can be tuned by weaving different numbers of modified cathode and anode fibers, respectively.

Titanium wires with diameters of approximately 100 μm were chosen as the substrate to make the modified cathode fibers. The modified cathode fibers were prepared using an all-solution dip-coating process that favored continuous and mass production with low cost and high efficiency (Fig. 2a). Briefly, the titanium wires were immersed into a sol–gel precursor solution of zinc acetate dehydrate and then thermally annealed to form ZnO nanocrystals as the cathode buffer layer. The active and hole transport layers were then sequentially deposited onto the ZnO layer by dip-coating with a poly{4,8-bis[(2-ethylhexyl)oxy]benzo[1,2-*b*:4,5-*b*′] dithiophene-2,6-diyl-*alt*-3-fluoro-2-[(2-ethylhexyl)carbonyl]thieno[3,4-*b*]thiophene-4,6-diyl}:[6,6]-phenyl C71 butyric acid methyl ester (PTB7:$PC_{71}BM$) blend solution and a poly(3,4-ethylenedioxythiophene):polystyrene sulfonate (PEDOT:PSS) solution, followed by thermal annealing to produce the modified cathode fiber. Fig. 2b represents a typical cross-sectional scanning electron microscopy (SEM) image, and optical microscope images of different layers of the cathode fiber are shown in Fig. S2.† A clear interface can be observed between the PTB7:$PC_{71}BM$ layer on the inside and the PEDOT:PSS layer on the outside, and each layer was ~150 nm in thickness.

The resulting modified cathode fibers were then woven with Ag-plated nylon yarn (Fig. S3†) as the anode using an industrial rapier loom to produce the polymer solar cell textile (Fig. 2c). Here, cotton threads were woven in both warp and weft directions to demonstrate the promise for practical applications, *i.e.*, the polymer solar cell may be easily made with other commercial yarns for real products such as clothes and tents. Of course, it was also good for other commercial yarns or without the commercial yarns. For a typical fabrication, the cotton threads and Ag-plated nylon yarns were first alternately fixed in the warp direction with certain widths, and the width depended on how many modules would be connected in series. After that, the cotton threads and modified cathode fibers were alternately woven in the weft direction, and the amount depended on how many modules would be connected in parallel. The anode and modified cathode fibers had close contact with each other in the vertical pattern, and the pitch of the anode fibers was around 500 μm (Fig. 2d). The resulting organic photovoltaic textiles were thin, with thicknesses of ~400 μm, and lightweight with densities of ~12 mg $cm^{-2}$.

During the fabrication of the polymer solar cell textiles, some processing conditions were optimized in order to achieve the best photovoltaic performance. The cathode buffer layer of ZnO nanocrystals plays an important role in electron collection and hole blocking. In addition, it significantly facilitates the adhesion of polymer layers in the following steps.[27,28] Therefore, controlling the morphology of the ZnO layer is important for tuning the contact quality so as to realize the full potential of the photovoltaic device. Here, the ZnO nanocrystal layer was prepared using a sol–gel method, and the sol concentration greatly affected the surface morphology of the ZnO layer and thus the device performance.[29] Fig. 2e–j show ZnO layers derived from sol concentrations of 0.05, 0.1, 0.2, 0.5, 1.0 and 2.0 M. The photovoltaic performances of the corresponding devices are compared in Table 1. The main photovoltaic parameters including $V_{oc}$, $J_{sc}$ and FF were all enhanced with increasing sol concentration from 0.05 to 0.5 M. Consequently, the power conversion efficiencies (PCEs) increased from 0.0023% to 1.62%. When the sol concentration further increased to exceed 0.5 M, the value of $V_{oc}$ slightly decreased, while both $J_{sc}$ and FF sharply decreased to clearly reduce the PCE from 1.62% to 0.27%.

By comparing the surface morphology of the ZnO layers with the corresponding device parameters, it was clear that there existed some relationship between the photovoltaic performance and the surface quality. For the ZnO layer derived from

 

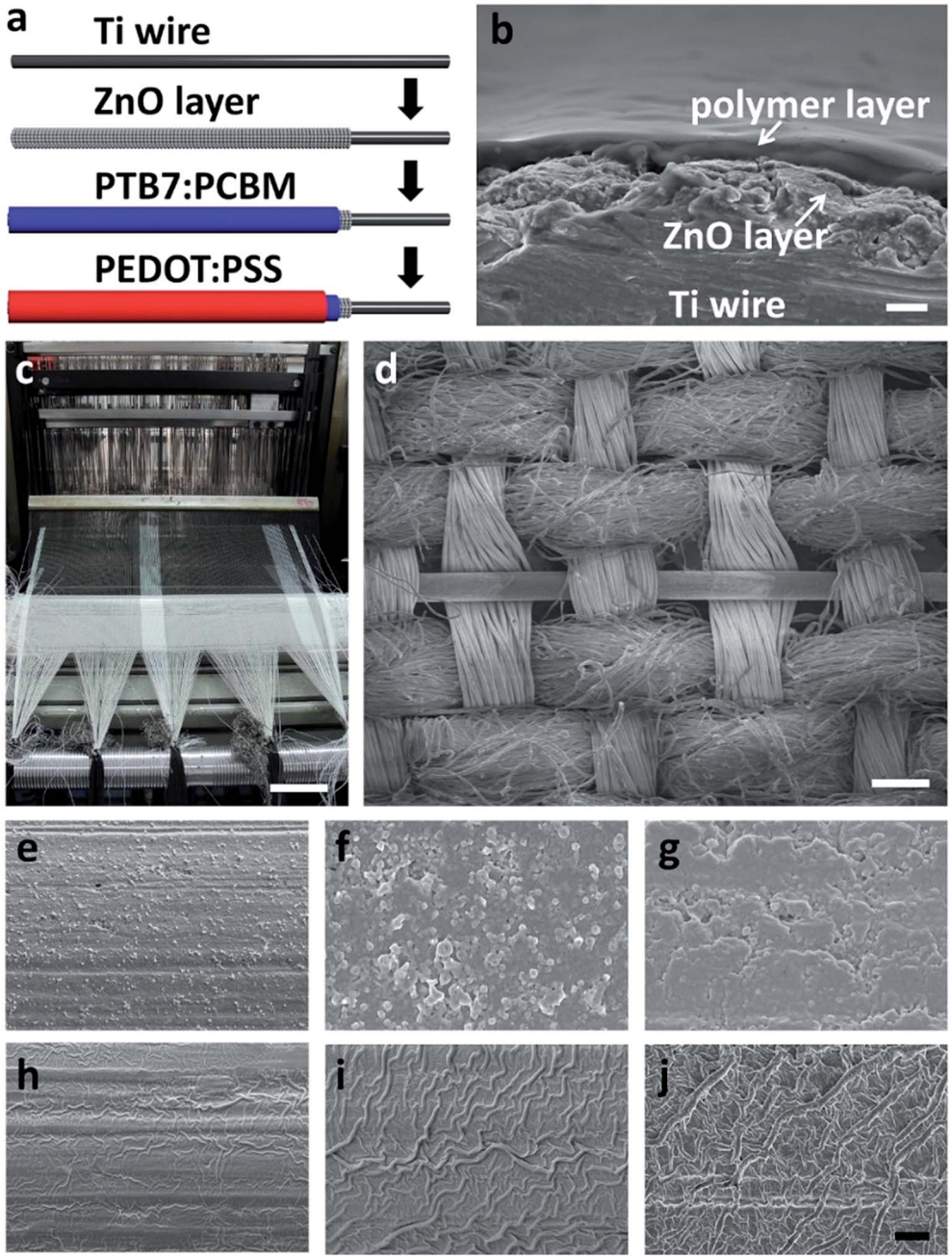


Fig. 2 (a) Schematic illustration of the fabrication process of the modified cathode fiber. (b) Cross-sectional SEM image of the modified cathode fiber. Scale bar, 500 nm. (c) Photograph of the production process of the polymer solar cell textile on a loom. Scale bar, 5 cm. (d) SEM image of the polymer solar cell textile. Scale bar, 200 μm. (e–j) SEM images of ZnO layers derived from sol concentrations of (e) 0.05, (f) 0.1, (g) 0.2, (h) 0.5, (i) 1.0 and (j) 2.0 M. Scale bar, 800 nm.

a sol concentration of 0.05 M, it was so dilute that only scattered ZnO nanoparticles were deposited on the surface, leading to a direct contact between the active layer and the titanium wire. It is well known that the ZnO buffer layer can lead to finely matched energy levels and good Ohmic contact between the active layer and the cathode layer, so the direct contact of these two layers without the ZnO layer would reduce the $V_{oc}$ to a great extent, because the reduction of the built-in potential caused an increment in leakage current and carrier recombination.[29] Besides, without the efficient electron extraction of the ZnO layer, the large energy barrier formed at the interface resulted in a high contact resistance, which can be observed from the high series resistance ($R_s$) of ~42 kΩ. With increasing sol concentration from 0.05 to 0.5 M, the increased coverage of the ZnO layer on the titanium wire surface could prevent direct contact between the active layer and the cathode, leading to increased $V_{oc}$ and decreased $R_s$, which produces higher $J_{sc}$ and FF. At a sol concentration of 0.5 M, the titanium wire surface was fully covered by a dense and homogenous ZnO layer in a nano-ripple pattern, which was also found in film polymer solar cells.[30] The

Table 1 The photovoltaic parameters of the polymer solar cell textile module with ZnO layers derived from different sol concentrations as the cathode buffer layer under illumination of AM 1.5 G, 100 mW $cm^{-2}$[a]

| $C$ (mol $L^{-1}$) | $V_{oc}$ (V) | $J_{sc}$ (mA $cm^{-2}$) | FF (%) | PCE (avg.) (%) | $R_s$[b] (kΩ) |
|---|---|---|---|---|---|
| 0.05 | 0.15 | 0.07 | 22.36 | 0.0023 (0.0018) | 42.4 |
| 0.1 | 0.24 | 2.68 | 22.64 | 0.14 (0.11) | 5.2 |
| 0.2 | 0.36 | 4.52 | 35.06 | 0.57 (0.48) | 2.4 |
| 0.5 | 0.48 | 7.39 | 45.88 | 1.62 (1.53) | 1.8 |
| 1.0 | 0.41 | 5.86 | 41.25 | 0.99 (0.82) | 2.3 |
| 2.0 | 0.40 | 2.37 | 28.58 | 0.27 (0.19) | 6.9 |

[a] The average values were calculated from at least five devices. [b] $R_s$ was measured and compared using the absolute resistance of devices with the same size.

nano-ripple ZnO layer provided a large interfacial area and intimate contact between the ZnO layer and the active layer, giving more efficient electron collection and lower $R_s$ values. As a result, the devices derived from the 0.5 M sol concentration demonstrated the highest PCE of 1.62%. Higher sol concentrations over 0.5 M produced coarse surfaces for the ZnO layers, and it was hard for the active layer solution to penetrate into the voids of the coarse surface due to a large difference in surface energy between the ZnO layer and the active layer, so the voids would lead to inferior contact and much higher $R_s$ with lower $J_{sc}$ and FF. Therefore, the surface quality of the ZnO layer is critical to the photovoltaic performance of the polymer solar cell textile.

In addition to the ZnO buffer layer, the concentration of PTB7:$PC_{71}BM$ solution also had a large impact on the thickness of the active layer and the device performance.[31] Here, a series of PTB7:$PC_{71}BM$ solutions with increasing concentrations from 10 to 30 mg $mL^{-1}$ were prepared as active layers. Since the layer thickness on the fiber device cannot be measured by a step profiler that is always used for thin film devices, here we obtained the average value from a number of cross-sectional SEM images of the coated fibers (Fig. S4†). The photovoltaic parameters of the resulting polymer solar cell textiles are compared in Table 2, and the corresponding structures are also provided in Fig. S5.† With the increasing concentrations of the PTB7:$PC_{71}BM$ solutions, the $V_{oc}$ values steadily increased while the FF values declined. At a solution concentration of 20 mg $mL^{-1}$, the highest $J_{sc}$of 7.31 mA $cm^{-2}$ was obtained to achieve the highest PCE of 1.6%. From the rising $R_s$ of the devices with increasing PTB7:$PC_{71}BM$ concentration, it can be speculated that too dilute solutions would probably produce ultrathin active layers with pores or traps, leading to leakage current and reduced $V_{oc}$, as well as insufficient light harvesting. Much higher concentrations would lead to large $R_s$ and more carrier recombination due to the thicker active layer. Besides, some other approaches that can effectively enhance the photovoltaic performances of thin film polymer solar cells have also been tried, like using different solvents to treat the active layer (Table S1 and Fig. S6†). Basically, the textile devices with an active layer prepared from chlorobenzene (CB) showed better performances than those from dichlorobenzene (DCB), but 1,8-diiodooctane (DIO) and methanol treatments demonstrated slight enhancements. It has been reported that for thin film polymer solar cells, these approaches can optimize the nanomorphology in the active layer, including phase separation, molecular packing and crystallization during the spin coating process, thus leading to improved performance.[32,33] However, for the fiber devices fabricated by dip coating, it is hard to optimize the nanomorphology of the active layer on the curved surface of the fiber, and very little enhancement was achieved using these approaches.

Table 2 The photovoltaic parameters of the polymer solar cell textile module with active layers derived from different concentrations of PTB7:$PC_{71}BM$ solutions under illumination of AM 1.5 G, 100 mW $cm^{-2}$[a]

| $C$ (mg $mL^{-1}$) | $V_{oc}$ (V) | $J_{sc}$ (mA $cm^{-2}$) | FF (%) | PCE (avg.) (%) | $R_s$[b] (kΩ) |
|---|---|---|---|---|---|
| 10 | 0.34 | 4.36 | 49.60 | 0.74 (0.65) | 1.6 |
| 15 | 0.43 | 6.57 | 47.57 | 1.34 (1.18) | 1.7 |
| 20 | 0.48 | 7.31 | 45.73 | 1.60 (1.52) | 1.9 |
| 25 | 0.50 | 5.22 | 43.33 | 1.13 (1.01) | 2.7 |
| 30 | 0.52 | 4.90 | 43.72 | 1.11 (0.93) | 2.8 |

[a] The average values were calculated from at least five devices. [b] $R_s$ was measured and compared using the absolute resistance of devices with the same size.

In addition to the processing conditions, the size of the modules that make up the textile is also crucial to the photovoltaic performance. Although the PCEs of the textile modules decreased with increasing module width from 1 to 10 cm, the generated absolute photocurrents increased almost linearly due to there being more light harvesting areas (Fig. 3a). Therefore, textile modules with a width of 10 cm were used for the following studies. Besides, some weaving parameters were also optimized to obtain better device performance, like the thickness and interval of the anode fibers (Ag-plate nylon yarns) (Tables S2 and S3†). Too thick anode fibers would block the incident sunlight and too large an interval would decrease the contact area of the two fiber electrodes. The circuit connection of the electrode fibers in the textile module was investigated first. For the parallel connection, the photocurrents of the photovoltaic textile module were increased linearly with an increasing number of connected modified cathode fibers, meanwhile the output voltage remained almost unchanged (Fig. 3b). For five modified cathode fibers connected in parallel, an $I_{sc}$ of 1.3 mA and a $V_{oc}$ of 0.4 V were achieved. For the series connection, the output voltages of the textile modules also increased linearly with increasing numbers of connected modified cathode fibers, while the photocurrent remained stable (Fig. 3c). For five modified cathode fibers connected in series, an $I_{sc}$ of 0.23 mA and a $V_{oc}$ of 2.1 V have been obtained. Therefore, the output power of the photovoltaic textile can be tuned according to the application requirements by varying the number of photovoltaic fibers connected in parallel or series.

The working stability of the photovoltaic textile is essential for its application. As shown in Fig. 3d, the PCE of the polymer solar cell textile retained over 85% of its initial value after 15 d in air. For stability under deformation, the bending test data shown in Fig. S7† show that the organic photovoltaic textile demonstrated stable performances with the PCE declining by

 

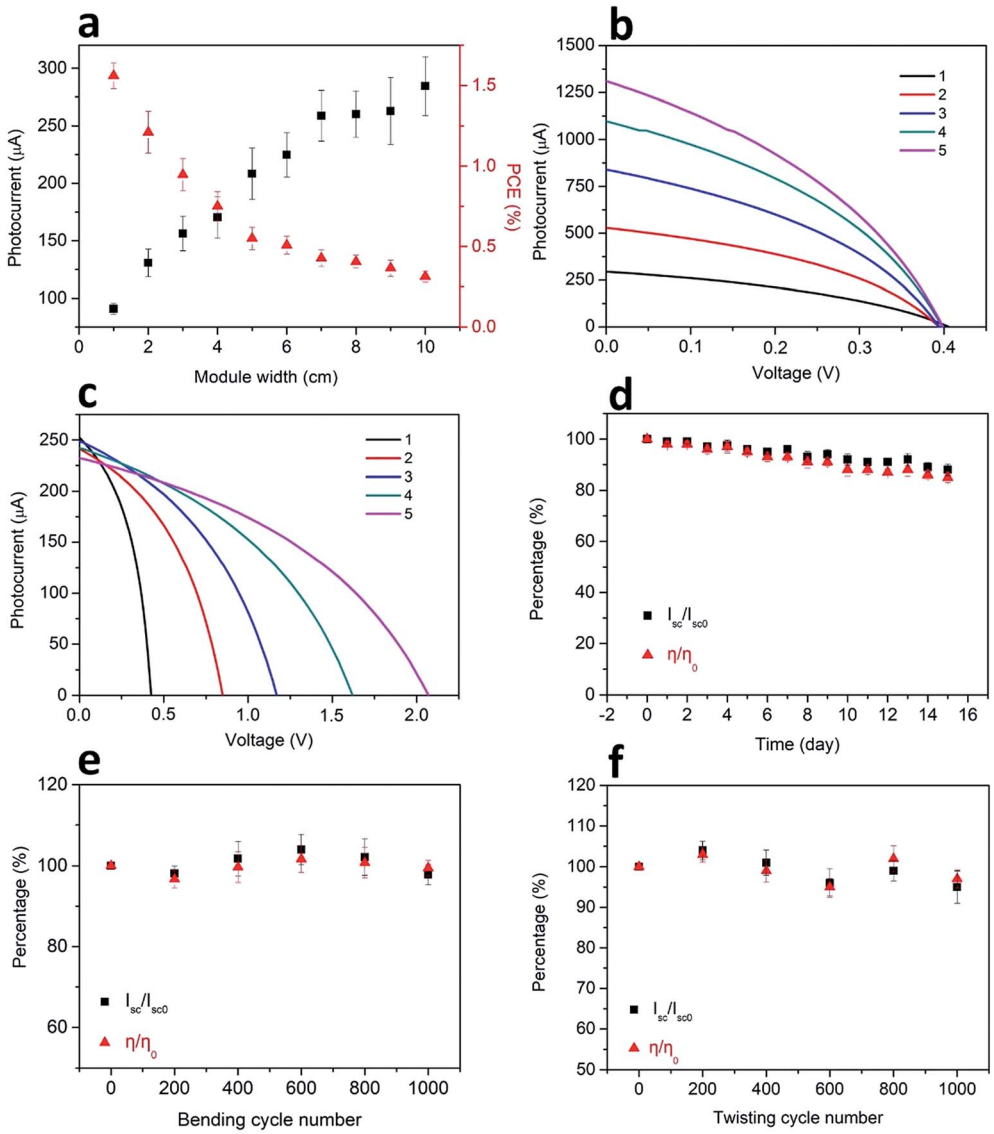


Fig. 3 (a) Photovoltaic performances of the polymer solar cell textile module with different widths. (b) and (c) Current–voltage curves of the textile modules with increasing numbers of modified cathode fibers connected in parallel and in series, respectively. (d) Dependence of photocurrent and PCE on time for the polymer solar cell textile in air. (e) and (f) Dependence of photocurrent and PCE on bending cycle number and twisting cycle number for the polymer solar cell textile. $I_{sc}/I_{sc0}$ and $\eta/\eta_0$ denote the photocurrent and PCE of the textile devices after and before deformation, respectively.

less than 15% even at a bending angle of 80°. The performance decline was probably due to the loose contact between the modified cathode and anode fibers with gradually increased bending angles, indicating that the performance could be recovered after release. As shown in Fig. 3e, the organic photovoltaic textile retained almost 100% of its initial performance after 1000 bending cycles. Also in the twisting test, the photovoltaic textile underwent 180° torsion and exhibited high stability during 1000 twisting cycles of this kind.

To demonstrate the practicality of the polymer solar cell textile as a power source for applications in fields such as wearable electronics, a piece of this photovoltaic textile was woven and used to drive an electronic device (Fig. 4a). The photovoltaic textile with a width of 25 cm was made from two modules connected in series, and each module consisted of five modified cathode fibers in parallel (Fig. 4b and c). The equivalent circuit of the photovoltaic textile is also shown in Fig. 4b, and it was further verified by the current–voltage curves shown in Fig. 4d. An $I_{sc}$ of 1.1 mA and a $V_{oc}$ of 0.83 V were achieved for the photovoltaic textile while one modified cathode fiber offered an $I_{sc}$ of 0.25 mA and a $V_{oc}$ of 0.42 V, which showed good correspondence with the equivalent circuit. Fig. 4e shows a digital watch that was powered up by the photovoltaic textile wrapped around the wrist under solar irradiation.

In summary, by designing an interlaced structure of cathode and anode fibers, we have realized the desired continuous and mass production of polymer solar cell textiles that has remained challenging in the past decade. The resulting photovoltaic

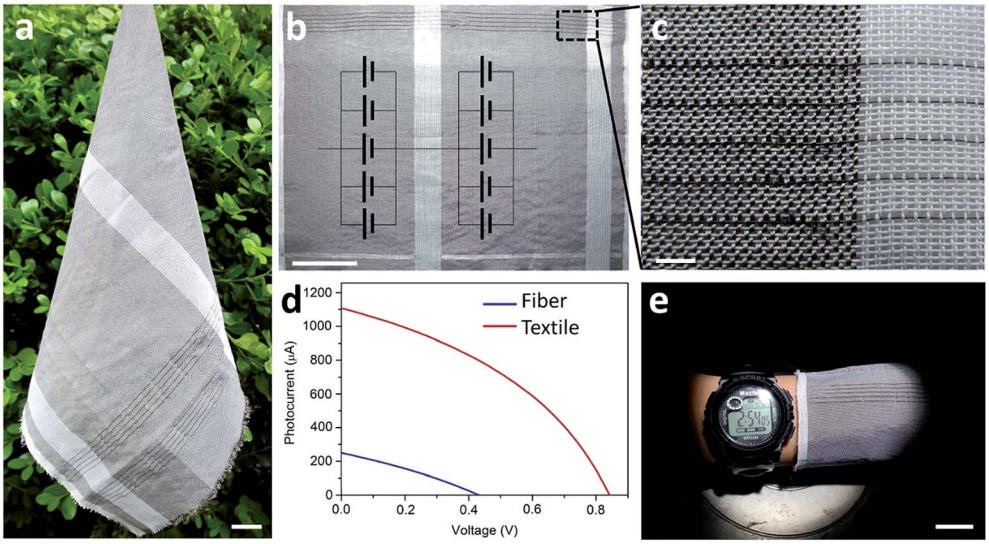


Fig. 4 (a) Photograph of a polymer solar cell textile. Scale bar, 2 cm. (b) and (c) Photographs of the photovoltaic textile at low and high magnifications, respectively (inset, the equivalent circuit of the photovoltaic textile). Scale bar, 5 cm for (b) and 3 mm for (c). (d) Photovoltaic performance of the textile device and one modified cathode fiber in the photovoltaic textile. (e) Demonstration of the photovoltaic textiles used to power an electronic watch under solar irradiation. Scale bar, 2 cm.

textiles were thin, lightweight, flexible and stable, affording them potential in a variety of applications, and the use of them to power wearable electronic devices has been demonstrated. In addition, the above fabrication can be easily scaled up using an industrial loom, which significantly promotes the commercialization of the organic photovoltaic textiles. This work may open up a new direction for the advancement of flexible power systems through the design of novel structures.

## Experimental section

### Materials

Ti wires (diameter of 127 μm, 99.99%) were purchased from Alfa Aesar. Zinc acetate dehydrate and ethanolamine were obtained from J&K Scientific. 2-Methoxyethanol, chlorobenzene, dichlorobenzene and 1,8-diiodooctane were ordered from Sigma-Aldrich. PTB7 and $PC_{71}BM$ were purchased from 1-Material. PEDOT:PSS PH1000 was obtained from Clevios. Ag-plated nylon yarns (Fig. S8†) were ordered from Qingdao Tianyin Textile Technology Co., Ltd. and Capstone FS-31 was purchased from Dupont.

### Fabrication of modified cathode fibers

The modified cathode fibers were prepared on Ti wires with a multiple dip-coating process, as shown in Fig. S9.† The coating solution was placed in a glass tube. Ti wire was clamped with a universal testing instrument (HY-0350, Hengyi) and then dipped into or pulled out of the coating solution. First, the Ti wire was sequentially washed with deionized water, acetone and isopropanol under sonication for 20 min each, then dried at 80 °C in an oven. ZnO nanocrystals were then coated on the Ti wire using a sol–gel method. The ZnO precursor solution was prepared by dissolving zinc acetate dehydrate and ethanolamine in 2-methoxyethanol (molar ratio of zinc acetate dehydrate and ethanolamine, 1 : 1), and the concentration of zinc acetate was varied from 0.05 to 2 M. The Ti wire was treated with UV ozone cleaner (PSD-UV4) for 15 min and then dip-coated into the ZnO precursor solution with a speed of 20 cm $min^{-1}$. After that, the Ti wire was annealed at 300 °C for 60 min to convert the zinc acetate to ZnO nanocrystals, and this procedure was repeated three times. The two polymer layers were dip-coated onto the modified Ti wire in sequence. The treated Ti wire was dipped into the solution of PTB7 and $PC_{71}BM$ for 5 min and then pulled out at a speed of 20 cm $min^{-1}$, followed by annealing at 150 °C for 10 min in a glovebox. The weight ratio of PTB7 and $PC_{71}BM$ was 1 : 1.5 with the concentration of PTB7 varied from 10 to 30 mg $mL^{-1}$. CB, DCB, CB:DIO (3 vol%) and DCB:DIO (3 vol%) were used as the solvent. For the methanol treatment, the PTB7:$PC_{71}BM$ coated fibers were dipped into methanol, pulled out quickly, and then kept at 25 °C for 5 min. After that, a mixture of PEDOT:PSS aqueous solution and fluorinated surfactant (Capstone FS-31, volume ratio of 200/1) was coated onto the PTB7:$PC_{71}BM$ layer at a speed of 20 cm $min^{-1}$, followed by annealing at 150 °C for 10 min.

### Fabrication of the polymer solar cell textile

The photovoltaic textile was made in plain weave on a rapier loom using traditional weaving technology (Tong Yuan Textile Machinery Co., Ltd, 40 cm in width). As shown in Fig. S10,† the cotton threads and Ag-plated nylon yarns were alternately fixed in the warp direction with certain widths. The width depended on the length of the modified cathode fibers and number of modules connected in series. The cotton threads and modified cathode fibers were then woven in the weft direction, and the amount depended on the number of modules connected in

 

parallel. A piece of photovoltaic textile with a size of $25 \times 50$ cm$^2$ was cut off as the sample. The effective area for the calculation of the PCE was obtained from the projected area of the organic photovoltaic textile. For the device performance characterization, the ends of the Ag-plated nylon yarns were connected with silver paste and then connected to the external facility to record the *J–V* curves of the photovoltaic textile.

### Characterization

The *J–V* curves of the photovoltaic textiles were recorded using a Keithley 2400 Source Meter under the illumination (100 mW cm$^{-2}$) of simulated AM1.5 solar light from a solar simulator (Oriel-Sol3A 94023A equipped with a 450 W Xe lamp and an AM1.5 filter). The surface morphology was characterized using scanning electron microscopy (S-4800, Hitachi).

## Conflicts of interest

There are no conflicts to declare.

## Acknowledgements

This work was supported by MOST (2016YFA0203302), NSFC (21634003, 51573027, 51403038, 51673043, 21604012, 21503079), STCSM (16JC1400702, 17QA1400400, 15XD1500400, 15JC1490200), SHMEC (2017-01-07-00-07-E00062) and the China Postdoctoral Science Foundation (2017M610223, 2018T110334).

## References

1 Q. Xue, J. Sun, Y. Huang, M. Zhu, Z. Pei, H. Li, Y. Wang, N. Li, H. Zhang and C. Zhi, *Small*, 2017, **13**, 1701827.
2 H. Nishide and K. Oyaizu, *Science*, 2008, **319**, 737–738.
3 W. Weng, P. Chen, S. He, X. Sun and H. Peng, *Angew. Chem., Int. Ed.*, 2016, **55**, 6140–6169.
4 J. Ren, Y. Zhang, W. Bai, X. Chen, Z. Zhang, X. Fang, W. Weng, Y. Wang and H. Peng, *Angew. Chem., Int. Ed.*, 2014, **53**, 7864–7869.
5 Y. Zhang, W. Bai, X. Cheng, J. Ren, W. Weng, P. Chen, X. Fang, Z. Zhang and H. Peng, *Angew. Chem., Int. Ed.*, 2014, **53**, 14564–14568.
6 M. Stoppa and A. Chiolerio, *Sensors*, 2014, **14**, 11957–11992.
7 N. Zhang, J. Chen, Y. Huang, W. Guo, J. Yang, J. Du, X. Fan and C. Tao, *Adv. Mater.*, 2016, **28**, 263–269.
8 P. Chen, Y. Xu, S. He, X. Sun, S. Pan, J. Deng, D. Chen and H. Peng, *Nat. Nanotechnol.*, 2015, **10**, 1077–1083.
9 D. J. Lipomi, B. C. K. Tee, M. Vosgueritchian and Z. Bao, *Adv. Mater.*, 2011, **23**, 1771–1775.
10 T. F. O'Connor, A. V. Zaretski, B. A. Shiravi, S. Savagatrup, A. D. Printz, M. I. Diaz and D. J. Lipomi, *Energy Environ. Sci.*, 2014, **7**, 370–378.
11 M. Kaltenbrunner, M. S. White, E. D. Głowacki, T. Sekitani, T. Someya, N. S. Sariciftci and S. Bauer, *Nat. Commun.*, 2012, **3**, 770.
12 Y. Li, G. Xu, C. Cui and Y. Li, *Adv. Energy Mater.*, 2018, **8**, 1701791.
13 W. Song, X. Fan, B. Xu, F. Yan, H. Cui, Q. Wei, R. Peng, L. Hong, J. Huang and Z. Ge, *Adv. Mater.*, 2018, **30**, 1800075.
14 S. Zhang, Y. Qin, J. Zhu and J. Hou, *Adv. Mater.*, 2018, **30**, 1800868.
15 N. Espinosa, M. Hosel, D. Angmo and F. C. Krebs, *Energy Environ. Sci.*, 2012, **5**, 5117–5132.
16 G. Li, R. Zhu and Y. Yang, *Nat. Photonics*, 2012, **6**, 153–161.
17 Z. Zhang, M. Liao, H. Lou, Y. Hu, X. Sun and H. Peng, *Adv. Mater.*, 2018, **30**, 1704261.
18 H. J. Park, M. G. Kang, S. H. Ahn and L. J. Guo, *Adv. Mater.*, 2010, **22**, E247–E253.
19 X. Gu, Y. Zhou, K. Gu, T. Kurosawa, Y. Guo, Y. Li, H. Lin, B. C. Schroeder, H. Yan, L. F. Molina, C. J. Tassone, C. Wang, S. C. B. Mannsfeld, H. Yan, D. Zhao, M. F. Toney and Z. Bao, *Adv. Energy Mater.*, 2017, **7**, 1602742.
20 A. K. Yetisen, H. Qu, A. Manbachi, H. Butt, M. R. Dokmeci, J. P. Hinestroza, M. Skorobogatiy, A. Khademhosseini and S. H. Yun, *ACS Nano*, 2016, **10**, 3042–3068.
21 Z. Zhang, Z. Yang, Z. Wu, G. Guan, S. Pan, Y. Zhang, H. Li, J. Deng, B. Sun and H. Peng, *Adv. Energy Mater.*, 2014, **4**, 1301750.
22 D. Liu, M. Zhao, Y. Li, Z. Bian, L. Zhang, Y. Shang, X. Xia, S. Zhang, D. Yun, Z. Liu, A. Cao and C. Huang, *ACS Nano*, 2012, **6**, 11027–11034.
23 M. R. Lee, R. D. Eckert, K. Forberich, G. Dennler, C. J. Brabec and R. A. Gaudiana, *Science*, 2009, **324**, 232–235.
24 Z. Zhang, X. Li, G. Guan, S. Pan, Z. Zhu, D. Ren and H. Peng, *Angew. Chem., Int. Ed.*, 2014, **53**, 11571–11574.
25 T. Chen, L. Qiu, Z. Yang and H. Peng, *Chem. Soc. Rev.*, 2013, **42**, 5031–5041.
26 W. Gao, S. Emaminejad, H. Y. Y. Nyein, S. Challa, K. Chen, A. Peck, H. M. Fahad, H. Ota, H. Shiraki, D. Kiriya, D.-H. Lien, G. A. Brooks, R. W. Davis and A. Javey, *Nature*, 2016, **529**, 509–514.
27 Z. Liang, Q. Zhang, L. Jiang and G. Cao, *Energy Environ. Sci.*, 2015, **8**, 3442–3476.
28 Y. Sun, J. H. Seo, C. J. Takacs, J. Seifter and A. J. Heeger, *Adv. Mater.*, 2011, **23**, 1679–1683.
29 Z. Liang, Q. Zhang, O. Wiranwetchayan, J. Xi, Z. Yang, K. Park, C. Li and G. Cao, *Adv. Funct. Mater.*, 2012, **22**, 2194–2201.
30 N. Sekine, C.-H. Chou, W. L. Kwan and Y. Yang, *Org. Electron.*, 2009, **10**, 1473–1477.
31 C. Duan, F. Huang and Y. Cao, *Polym. Chem.*, 2015, **6**, 8081–8098.
32 S. Guo, W. Wang, E. M. Herzig, A. Naumann, G. Tainter, J. Perlich and P. Muller-Buschbaum, *ACS Appl. Mater. Interfaces*, 2017, **9**, 3740–3748.
33 S. Guo, B. Cao, W. Wang, J. F. Moulin and P. Muller-Buschbaum, *ACS Appl. Mater. Interfaces*, 2015, **7**, 4641–4649.